Temperature-Controlled Rotational Epitaxy of Graphene

Karim M. Omambac,*[‡,#] Hichem Hattab,[†] Christian Brand,[†] Giriraj Jnawali,[†,∥] Alpha T. N'Diaye,[‡,⊥] Johann Coraux,[§] Raoul van Gastel,[§,▽] Bene Poelsema,[§] Thomas Michely,[†] Frank-Joachim Meyer zu Heringdorf, and Michael Horn-von Hoegen

[†]Faculty of Physics and Center for Nanointegration Duisburg-Essen (CENIDE), University of Duisburg-Essen, Lotharstraße 1, 47057 Duisburg, Germany

[‡]Institute of Physics II, University of Cologne, Zülpicher Straße 77, 50937 Cologne, Germany

[§]Physics of Interfaces and Nanomaterials, MESA+ Research Institute, University of Twente, Drienerlolaan 5, 7522 NB Enschede, The Netherlands

ABSTRACT: When graphene is placed on a surface, the periodic structures within the layers and moirésuperlattices form. Small lattice rotatio the two materials in contact strongly modify the parameter, upon which many electronic, vibra chemical properties depend. While precise adjust relative orientation in the degree- and subdegree- achieved via careful deterministic transfer of graphene, we report on the spontaneous reorientation of graphene on a metallic substrate, Ir(111). We find that selecting a substrate temperature between 1530 and 1000 K during the growth of graphene leads to distinct relative rotational angles of 0°, ± 0.6°, ±1.1°, and ±1.7°. When modeling the moirésuperlattices as two-dimensional coincidence networks, we can ascribe the observed rotations to favorable low-strain graphene structures. The dissimilar thermal expansion of the substrate and graphene is regarded as an effective compressive biaxial pressure that is more easily accommodated in graphene by small rotations rather than by compression.

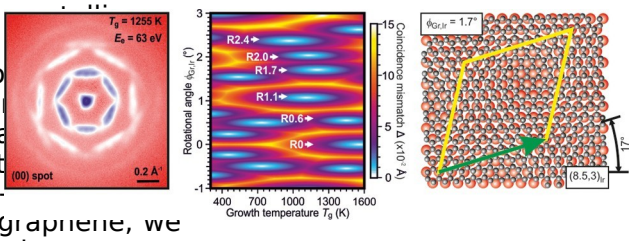

KEYWORDS: *graphene, strain-relief, moire´,iridium, thermal expansion*

In most future applications, graphene will have to be supported either by a substrate or another two-dimensional (2D) material.[1] Since the lattice parameters of the graphene and the neighboring materials are usually different, lateral modulations in the stacking configuration will result. These modulations are described as moirélattices, and their properties are determined by the rotational angle, which also defines the resulting strain state of the graphene.[2−4] Controlling the moirépattern's structural parameters constitutes a major yet important challenge[5] since the parameters of the moirépattern cause fundamental changes to the control the properties of the 2D material. We use high- resolution low-energy electron diffraction to study the moiré patterns formed between graphene and Ir(111). In comparison to local probes, diffraction is excellently suited to determine the angular distribution of rotated domains, as it averages over a large surface area. In earlier studies of graphene on Ir(111), large angles of rotation have been found at different growth temperatures, which have been studied extensively in the past.[16,17]

In contrast, here we report distinct rotational angles of 0°, ±

properties of graphene. Known examples for the influence of the moirépattern are the amplitude and energy range of moiré-induced electronic mini-gaps,[6,7] superlattice Dirac cones[8] in graphene, the energy range of Van Hove singularities in twisted bilayer graphene,[9,10] the Hofstadter butterfly spectrum in graphene on hexagonal boron nitride,[11,12] and correlated electron phenomena in twisted bilayer graphene.[13−15] In all these examples, the interaction between graphene and the support is sufficiently weak to maintain the graphene's genuine 2D properties, while it can be shown that the properties are modified by the presence of the moirésuperstructure.

Here, we address the question whether engineering of the moirépattern in a high-quality epitaxially grown graphene or 2D related material through manipulation of the rotational angle is possible. Such engineering might provide a strategy to

0.6°, ±1.1°, and ±1.7° as the growth temperature decreased from 1530 to 1000 K. We explain the observed rotational angles within a basic model describing the 2D in-plane coincidence of the substrate and graphene lattice. Justified by the results of Hattab et al.,[18] our model accounts for the varying lattice parameter of Ir(111) compared to an essentially constant graphene lattice parameter, as the growth temperature changes. The distinct thermal behavior of the two materials effectively imposes a biaxial pressure exerted on the graphene layer, which induces a rotation rather than compression. This has lately been referred to as rotational epitaxy.[19]

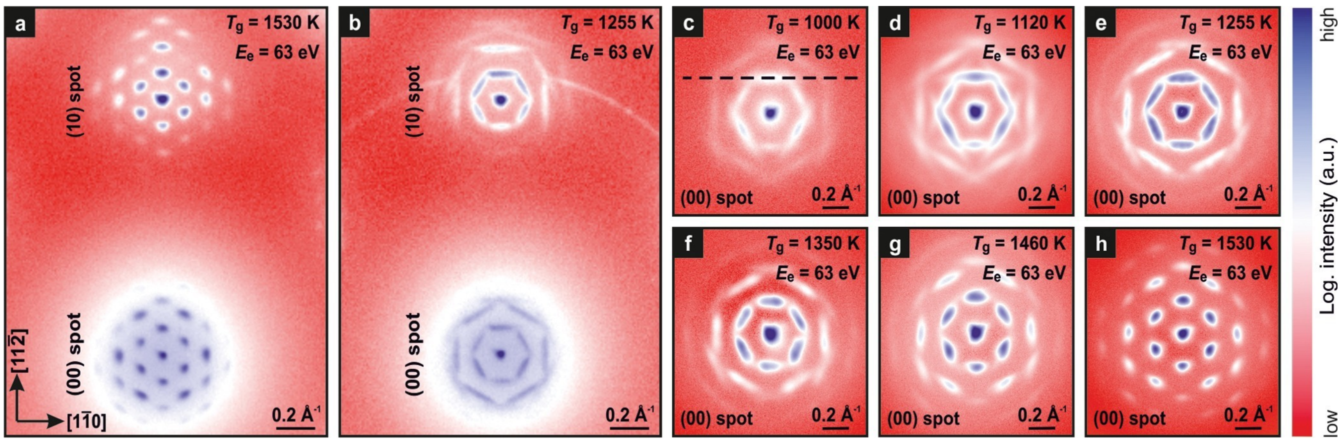

Figure 1. Room-temperature SPA−LEED patterns at different growth temperatures T_g for E_e = 63 eV. (a,b) Overview patterns for growth at 1530 and 1255 K, respectively. (c−h) Close-up patterns of the (00) spot at different growth temperatures between 1000 and 1530 K with subtracted background to reveal details of each spot. In (c) the direction of the line profiles shown in Figure 2a is marked by the dashed black line.

Experimental Section. Preparation of samples and experiments were performed in an ultrahigh vacuum (UHV) chamber with a base pressure of 1 × 10^{-10} mbar. The UHV chamber is equipped with a chemical vapor deposition reactor for preparation. Spot profile analysis−low energy electron diffraction (SPA−LEED) was used for characterizing the orientation of the graphene layer. SPA−LEED provides superior resolution in terms of reciprocal space and signal-to-noise ratio in comparison to conventional optical LEED systems.[20,21] A well-oriented Ir(111) substrate was prepared by repeated sputter annealing cycles until the full width at half-maximum (FHWM) of the diffraction spots was limited by the instrumental resolution of ∼1% Brillouin zone. On the Ir(111) surface, graphene layers were grown using thermal catalytic decomposition[22] of ethylene (C_2H_4) at a pressure of 5 × 10^{-6} mbar and substrate temperatures between 1000 and 1530 K (reached using electron bombardment of the backside of the sample). The sample temperature was determined using an Impac IGA 10 infrared pyrometer. The decomposition of C_2H_4 is only effective in the presence of bare Ir(111) so graphene growth is self-limited[22] to a single layer. Under the conditions used here, the surface is completely covered with graphene after less than 1 min of exposure with C_2H_4. SPA−LEED probes a surface area of the order of 1 mm2, and thus, the diffraction pattern is averaged across this surface area. All SPA−LEED patterns and line profiles were recorded at room temperature, after the sample has been cooled down from growth temperature.

Results and Discussion. Figure 1 shows SPA−LEED patterns at an electron energy of E_e = 63

$k_{moiré} = k_{Gr} - k_{Ir}$.[2,3,24] The position of the moiréspots is thus strongly dependent on even very small variations of the graphene lattice parameter[17] or rotations[25,26] the moiréspots act as a "magnifying glass" to detect strains and rotated domains. Figure 1b shows the same segment of the reciprocal space after preparation of graphene at a lower temperature of 1255 K. It is known that at such low growth temperatures graphene forms large-angle rotational domains on the surface,[16,17,27,28] and these domains are reflected in a faint ring of diffracted intensity, which is centered around the (00) spot and intersects the (10) spot. Also, unlike in Figure 1a, the moiréspots in Figure 1b are substantially elongated, similarly observed by Usachov et al.[29] Figure 1c−h shows the temperature dependence of the spot elongation around the (00) spot. With an increasing growth temperature, the elongated character is progressively lost.

eV. Figure 1a,b show sections of the reciprocal space including the (00) spot and the first integer order spot (10) for growth at 1530 and 1255 K, respectively. In Figure 1a the graphene layer is not rotated with respect to the Ir substrate (R0 phase); still, both Ir(111) integer order spots are surrounded by distinct satellite spots that arise from the moirépattern of the graphene layer and the Ir(111) substrate.[17,23] The spot spacing between the satellites is determined by the lattice parameter difference of graphene and Ir of ~10%.[17,18] These moiréspots are clearly observed up to fourth order in the false-color plot, reflecting the long-range order of the epitaxially grown graphene on the Ir(111) substrate. The positions of the moiréspots can be determined as a function of the graphene and Ir(111) unit cell vectors as

Figure 2 summarizes an analysis of the first order moiré spots surrounding the (00) spot, along the dashed black line shown in Figure 1c. Figure 2a shows a stack of line profiles recorded after growth at different temperatures. The profiles have been vertically shifted, and the growth temperature increases from bottom to top. The features marked “B” and “C” in the profiles simply originate from intersections with other first and higher-order moiréspots and do not warrant further discussion. We will instead discuss the central features “A” and “R0”, which provide new information about the morphology of the graphene layer. With increasing growth temperature these features become sharper. At intermediate growth temperatures of 1255−1350 K not only a broadening of “A” is observed but also a fine structure of two or three distinct and distinguishable diffraction peaks can be identified. These peaks each correspond to small-angle rotations with respect to the Ir(111) lattice (amplified by the aforementioned “magnifying glass” effect), meaning the graphene layer comprises small-angle rotational domains.

The intensity profiles of the moiréspots in Figure 2a reflect the angular distribution function of rotated domains in the graphene layer.[17,28] Figure 2d illustrates the relevant angles and lattice vectors that result in the formation of rotated moiré patterns. For each rotated domain, the rotational angle $\phi_{Gr,Ir}$ relative to the Ir substrate can be determined with extremely high accuracy from the experimental splitting of the first order moiréspots ($\delta k_{,[11\bar{2}]}$ $\delta k_{,[1\bar{1}0]}$) relative to the (00) spot. The

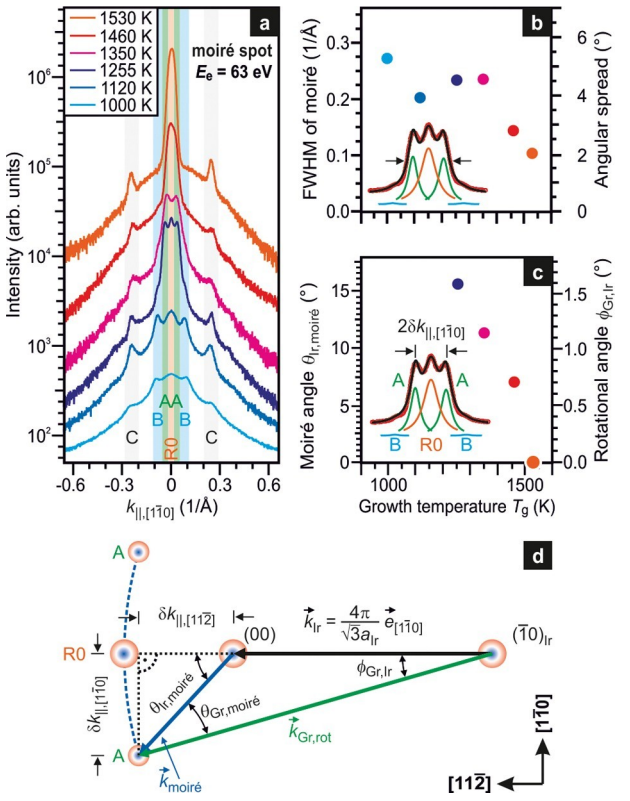

Figure 2. Moiréspot analysis. (a) High-resolution SPA−LEED line profiles reflecting the angular distribution of rotated domains. The line profiles have been recorded for different growth temperatures T_g and were taken along the elongated direction of the first order moiré spots of the (00) spot as marked in Figure 1c. (b) fwhm of the entire moirépeaks "R0" and "A" at different temperatures. (c) Observed rotational angle $\phi_{Gr,Ir}$ and moiréangle $\theta_{Ir,moiré}$as a function of graphene formation temperature. (d) Schematic diagram of the reciprocal lattice vectors of rotated graphene $k_{Gr,rot}$ and Ir k_{Ir} along with the rotational angle $\phi_{Gr,Ir}$, and the moiréangles $\theta_{Ir,moiré}$and $\theta_{Gr,moiré}$with respect to Ir(111) substrate and graphene, respectively (the positions of the spots are shifted for better visibility).

experimental values of $\delta k_{\parallel,[1\bar{1}0]}$ can be extracted directly from Figure 2a. The moiréangle $\theta_{Ir,moiré}$can also be derived by considering the two triangles in Figure 2d as

$$\tan\theta = \frac{\delta k_{,[1\bar{1}0]}}{} = \sin\phi_{Gr,Ir}$$

is present at 1530 K, resulting in a high-quality well-ordered graphene layer without additional rotated domains.

The rotational angles $\phi_{Gr,Ir}$ of the components of the "A" feature are determined using eq 2 (see Figure 2c). Fitting the line profiles in Figure 2a with Gaussian peaks, we are able to extract distinct rotational angles for growth temperatures of 1255 and 1350 K. For the growth at 1255 K, we observe three peaks at $\phi_{Gr,Ir} = \pm 1.7°$ and $\phi_{Gr,Ir} = 0°$, respectively, while for the growth at 1350 K, we only observe two peaks at $\phi_{Gr,Ir} = \pm 1.1°$ without any contribution of the R0 phase. The line profile of the graphene layer grown at 1460 K does not show distinct peaks. Instead, the central part of the moiréspot is significantly broadened in comparison with the other growth temperatures. This broadening suggests that the moiréspot actually consists of three overlapping contributions, wherein there is a coexistence of small-angle rotated domains with $\phi_{Gr,Ir} = \pm 0.6°$ and $\phi_{Gr,Ir} = 0°$. For a graphene formation temperature of 1530 K, we finally find the R0 phase only. We note that for lower growth temperatures (1120 and 1000 K), we do not observe any rotational angles between the intersections "B" from other first order moiréspots except the R0 phase. Nonetheless, from the SPA−LEED patterns at 1255 K shown in Figure 1b,e, we know that domains with larger rotational angles must be present.

To explain the observed rotational angles and their monotonic decrease with increasing growth temperature, we performed a simple 2D in-plane coincidence site lattice (CSL) analysis without concerning substrate−graphene interaction and graphene lattice undulation: we constructed rigid graphene and Ir lattices with the appropriate lattice parameters. The simulation cell consisted of 10 × 10 graphene unit cells and a larger Ir(111) lattice. The thermal expansion of the Ir lattice parameter[32,33] was considered for elevated formation temperatures. In the relevant growth temperature range between 1000 and 1550 K, the Ir lattice parameter increases by 0.4%. We modeled the graphene layer using the commonly accepted value of $aGr = 2.465$ Å for unstrained graphene,[34−36] which is, just like graphite,[37,38] temperature independent[39] in the temperature range considered here. We then rotated the graphene layer with respect to the Ir(111) lattice around a high-symmetry site in small increments of 0.01° while keeping the vertical distance between the graphene plane and the Ir surface constant. Based on the work by Merino et al.[40] we refer to the minimum value of the distance between all the C and Ir

$$\delta k_{Ir,moir} = \text{atoms}\left(\cos\left(-\frac{a_{Gr}}{a_{Ir}(T)}\right)\right) \quad (1)$$

where $a_{Ir}(T)$ and a_{Gr} are the lattice parameters of Ir(111) and graphene, respectively. From Figure 2d we also derive $\theta_{Ir,moiré} = \phi_{Gr,Ir} + \theta_{Gr,moiré}$.[31]

For small angles $\phi_{Gr,Ir}$ and $\theta_{Ir,moire}$, eq 1 simplifies to

$$\phi_{Gr,Ir} \cong \sqrt{3}\left(1 - \frac{a_{Gr}}{a_{Ir}(T)}\right)\cdot\tan\theta_{Ir,moir} \quad (2)$$

To further analyze the moiréspots, we first discuss the overall fwhm of the “A” feature as a whole (see Figure 2b). Our fit includes the $\phi_{Gr,Ir}$ = 0° component (R0 phase) and the two side peaks. This fwhm is a measure of the overall spread of the angular distribution of the rotated domains. A decrease of the fwhm is observed for increasing growth temperatures, indicating a reduction of the angular distribution of the rotational angles $\phi_{Gr,Ir}$. Eventually, only the oriented R0 phase except the atoms at the high-symmetry site at the origin of rotation) as the coincidence mismatch Δ, which is a function of the rotational angle. Despite the simplicity of the definition of Δ, we can nevertheless determine the occurrence of several preferential orientations $\phi_{Gr,Ir}$ versus growth temperature by varying the Ir surface lattice parameter.

The result of the simulation is shown in Figure 3a where the coincidence mismatch Δ is color-coded as a function of the growth temperature and the rotational angle $\phi_{Gr,Ir}$. While areas reflect minima of Δ of the stable rotational unstable configurations. Within the analyzed temperature regime, small-angle rotational domains R0, R0.6, R1.1, R1.7, R2.0, and R2.4 are found. All these represent local minima of Δ across a few 100 K. For 1530 K the minimum at $\phi_{Gr,Ir}$ = 0° marks a simple coincidence ratio of 10 graphene unit cells on nine Ir(111) unit cells (10:9). Decreasing the growth temperature to 1460 K, we find two primary minima (see curve at 1460 K of Figure 3b), which indicate the coexistence

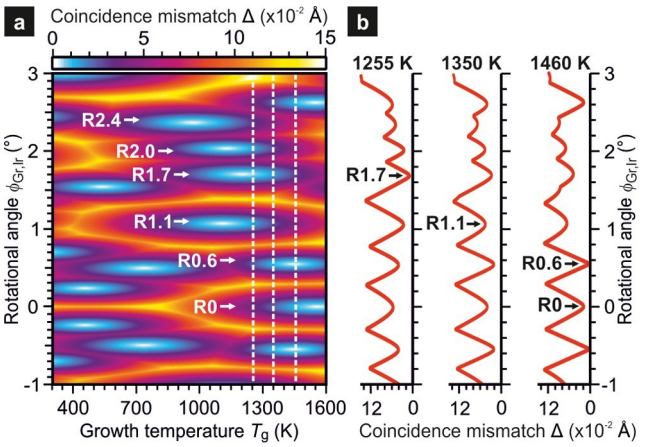

Figure 3. Coincidence site lattice analysis. (a) Two-dimensional representation of the coincidence mismatch Δ as a function of the rotational angle $\phi_{Gr,Ir}$ and the growth temperature. White color indicates the vanishing of Δ and denotes the existence of a coincidence site within the simulated lattice. Blue, red, and yellow colors indicate increasing values of Δ, indicative for conditions, where the graphene and Ir lattices do not exhibit coincidence lattice sites without straining the graphene layer. (b) Stability curves that correspond to coincidence phases with an angular orientation that accumulate the minimum value of Δ for specific temperatures.

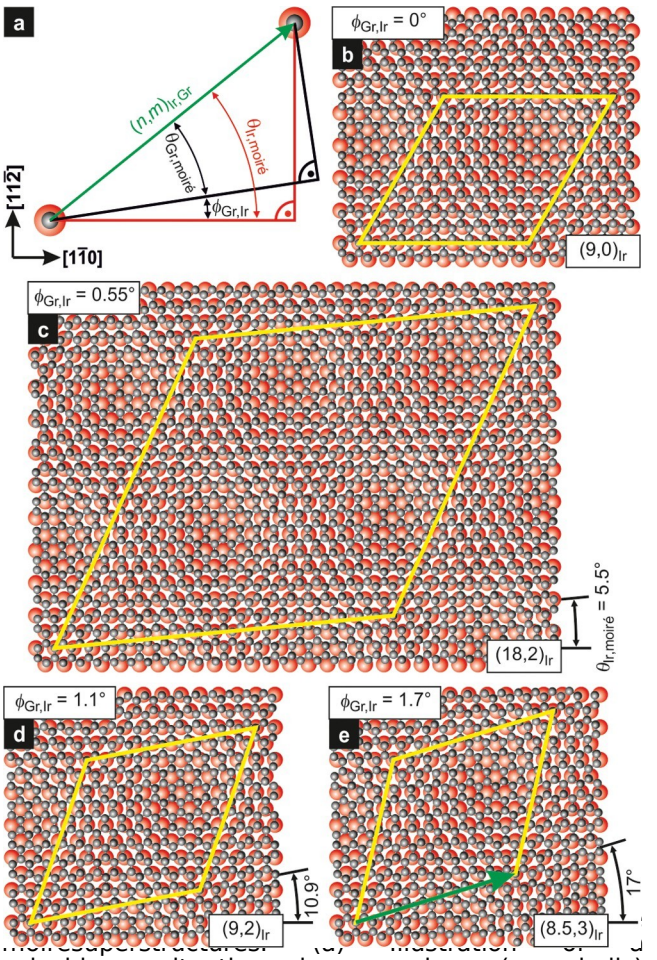

coincidence situation where graphene (gray balls) and Ir(111) substrate (red balls) describing coincidence vector $(n,m)_{Ir,Gr}$ along with the rotational angle $\phi_{Ir,Gr}$ and the moiréangles $\theta_{Ir,moiré}$and $\theta_{Gr,moiré}$. (b−e) Moirésuperstructures for small rotational angles $\phi_{Gr\ Ir}$ (calculated by eq 2), which read 0°, +0.6°, +1.1°, and +1.7° for panels b−e, respectively. $(n,m)_{Ir,Gr}$ is exemplarily shown in (e) for the R1.7 phase with n_{Ir} = 8.5 and m_{Ir} = 3 as the green-colored arrow.

of two phases of differently rotated domains (R0 and R0.6), with the R0.6 phase being dominant. This result from the model nicely matches the experimental observation. At 1350 K the simulation in Figure 3b shows four prominent minima at rotational angles $\phi_{Gr,Ir}$ that correspond to the R0.6 phase for the deepest minimum, and the R0, R1.1, and R1.7 phases for the other minima. In SPA−LEED we only observe the R1.1 phase at this temperature. Further decrease of the growth temperature results in an increase of Δ for the R0 phase, such that other rotated domains (R0.6, R1.1, and R1.7) become more favorable. Particularly at 1255 K we obtain the minimum Δ for the R1.7 phase consistent with the observations made by SPA−LEED in Figure 2c.

A real space model of the oriented R0 phase with 10:9 coincidence ratio of the graphene and Ir lattices is sketched in Figure 4b, while the commensurate rotated R0.6, R1.1, and R1.7 phases are shown in Figure 4c−e. While the graphene lattice is only rotated by a small rotational angle $\phi_{Gr,Ir}$, the moirépattern exhibits a larger rotational angle $\theta_{Ir,moire}$.As indicated in Figure 4a the moirémagnification also works in

$$\varepsilon_C = 1 - \frac{9}{\sqrt{4n_{Gr\,2} + 3m_{Gr\,2}}\sqrt{4n_{Ir\,2} + 3m_{Ir\,2}}} \quad (3)$$

By evaluating eq 3, we arrive at $\varepsilon_C = 0.27\%$ (as compared to the unstrained R0 commensurate real space.[30] In the following we will discuss the case of the R1.7 phase shown in Figure 4d as an example for all other rotational phases. It is coincident with a lateral translational vector of $n_{Ir} = 8.5$ Ir atom distances a_{Ir} along the $[1\bar{1}0]$-direction and $m_{Ir} = 3$ Ir atomic row distances $a_{Ir,row} = (\sqrt{3}/2)a_{Ir}$ along the perpendicular $[11\bar{2}]$-direction. Hence, the length of this so-called coincidence vector $(n,m)_{Ir}$ is given by $\frac{1}{4}\sqrt{n^2 + 3m^2}\cdot a_{Ir} = \sqrt{79}\cdot a_{Ir}$, which corresponds to the higher-order commensurate (HOC) structure $Ir(\sqrt{79} \times \sqrt{79})$ with respect to the Ir(111) substrate and $Gr(\sqrt{97} \times \sqrt{97})$ with respect to the graphene lattice.[41] This R1.7 coincidence structure of an unstrained graphene layer with $a_{Gr} = 2.465$ Å fits to the Ir lattice only if the Ir lattice parameter is reduced by

$$\varepsilon_L = 1 - \frac{a_{Ir}(1530\ \mathrm{K})}{a_{Ir}(T)} \quad (4)$$

which is $\varepsilon = 0.23\%$. Thus, the R1.7 phase becomes more favorable compared to the R0 phase because the graphene layer is less strained when it is rotated. Table 1 summarizes the considerations of coincidence vector, rotational angle, and strain for the observed small-angle rotated domains.

Our simulations suggest that, given Ir's thermal expansion, the R0 phase can only fulfill the coincidence of every 10th graphene unit cell on top of every ninth unit cell of the Ir(111) substrate at a particular growth temperature of 1530 K. Lower growth temperatures and maintaining an unstrained graphene lattice parameter result in a rotation of the graphene layer with

Table 1. Small-Angle Rotational Domains for Graphene on Ir(111)[a]

phase Ir	coincidence vector $(n,m)_i$ i = Gr	i = Ir	higher-order commensurate (HOC) structure	Moiréangle $\theta_{Ir,moiré}$	rot. angle $\phi_{Gr,Ir}$	relative change ε_L of Ir lattice parameter	relative coincidence mismatch ε_C	exp. growth temp. T
R0	(10,0)	(9,0)	$Gr(10 \times 10)/Ir(9 \times 9)$	0°	0°	–	–	1530 K
R0.6	(20,2)* (18,2)*		$Gr(\sqrt{403} \times \sqrt{403})$ $/Ir(\sqrt{327} \times \sqrt{327})$	5.5°	0.55°	0.06%	0.09%	1460 K
R1.1	(10,2) (9,2)		$Gr(\sqrt{103} \times \sqrt{103})$ $/Ir(2\sqrt{21} \times 2\sqrt{21})$	10.9°	1.07°	0.15%	0.34%	1350 K
R1.7	(9.5,3) (8.5,3)		$Gr(\sqrt{97} \times \sqrt{97})$ $/Ir(\sqrt{79} \times \sqrt{79})$	17.0°	1.70°	0.23%	0.27%	1255 K
				20.2°	2.03°	–	0.33%	–
R2.0	(18.5,7)*	(16.5,7)*	Gr(379×379)/Ir(309×309)	23.4°	2.36°	–	0.44%	–
R2.4	(9,4) (8,4)		$Gr(\sqrt{93} \times \sqrt{93})$ $/Ir(2\sqrt{19} \times 2\sqrt{19})$					

[a]Calculated coincidence vectors, HOC structure, Moiréand rotational angles, relative change of the Ir lattice parameter ε_L with respect to 1530 K, relative coincidence mismatch ε_C, and experimental growth temperature. The calculated results are compared to the HOC values using density functional theory based on first-principle calculations by Meng et al.[41] Asterisk (*) signifies the second order coincidence vector coordinates as shown exemplarily for the R0.6 phase in Figure 4c with a larger unit cell.

respect to the Ir(111) lattice to adopt other commensurability conditions. The tendency of forming rotational coincidences is a resemblance of the so-called rotational epitaxy that was introduced by Novaco and McTague[42] to account for similar small-angle rotations observed at first in 2D lattices of noble gas atoms deposited on graphite[19] and, later on, in many other systems including layers of alkali atoms or molecules on metal or graphite surfaces.[43−45] In these systems, the driving force for the rotation was the joint effect of (i) the increase of the adsorbate density at the 2D lattice (in our case an effective biaxial compressive stress) and (ii) the repulsion within the constituents of the lattice, forbidding excessive compressive strain. In the case of the self-limited growth of graphene grown at different temperatures on the Ir(111) surface, the amount of C atoms in the graphene layer does not change in absolute numbers but as a relative with respect to the Ir substrate. Indeed, the negligible thermal compression of the graphene lattice parameter in comparison with that of Ir(111)[32,33,38,39] effectively corresponds to an increase of the relative C atom density on Ir(111) as the growth temperature decreases, in other words, the buildup of an effective biaxial compressive rotations rather than by compressions of the graphene lattice. Within our coincidence site lattice model, we are able to reproduce our experimental results, and we find robust locking conditions of the rotated graphene with minima in the stability curve for the distinct commensurate small-angle rotational phases.

As our model is only sensitive to the strongest coincidence of C atoms in graphene with atoms of the topmost layer of the metal substrate, the binding,[49] at least locally, must exhibit covalent contributions instead of being only of the van der Waals type. Anticoincidence sites, however, naturally also exist in the moirélattice, and there the graphene-Ir atom distance is typically larger by 0.1−1 Å.[23,36,46] From the robust rotational locking conditions, we are furthermore able to estimate the lattice parameter of relaxed graphene on Ir(111) at the investigated growth temperatures. Considering the general assumption of small or negligible thermal expansion of graphene, we can conclude the room temperature lattice parameter $aGr/Ir(111) = 2.465 \pm 0.003$ Å for relaxed graphene on Ir(111).

stress. The resulting strain is relieved through the observed small-angle rotations rather than accommodated through isotropic compression.

Summary and Conclusions. During growth of graphene on Ir(111), islands with a variety of rotational angles are formed. Large-angle rotations on various substrates were already reported several years ago[16,40,48,49,52] and are believed to be formed due to kinetic limitations.[51] Here, we report a new class of small-angle rotations at distinct angles of ±0.8°, ±1.1°, and ±1.7°. While some of these have been predicted by density functional theory,[41] there was no experimental evidence for their existence until now. The presence of the particular angles we observe in the present study can be explained by strain minimization between the graphene layer and the Ir(111) substrate. As the growth temperature is decreased, the Ir lattice parameter shrinks while the graphene lattice parameter remains almost constant.[47] We argue that the significant reduction of the substrate's lattice parameter during growth at lower temperature imposes a biaxial

The existence of rotated domains with robust locking conditions for graphene on Ir(111) is similar to 2D lattices of noble gas or alkali atoms at the surface of graphite or metals, where increasing adatom density resulted in increasing compressive strain and a series of distinctly rotated domains.[19,43−45] This was referred to as rotational epitaxy.[42] In our version of rotational epitaxy, however, it is not a changing adatom density but the effective biaxial stress imposed by the substrate that causes the effect.

Our study emphasizes the important role of the substrate's temperature-dependent lattice parameter resulting in the formation of small-angle rotated domains. Depending on the interaction strength between the substrate and any epitaxially grown 2D materials,[50] we would expect the formation of similar thermodynamically stable small-angle rotational domains to be inevitable. However, the rotational epitaxy presented here may provide a route to achieve particular orientations in stacks of 2D materials, which

AUTHOR

INFORMATION

Corresponding Author

*E-mail: karim.omambac@uni-due.de.

ORCID

Karim M. Omambac: 0000-0002-5013-9567

Johann Coraux: 0000-0003-2373-3453

Frank-Joachim Meyer zu Heringdorf: 0000-0002-5878-2012

Present Addresses

‖(G.J.) College of Arts and Sciences, University of Cincinnati, 2700 Campus Way, Cincinnati, OH 45219, United States.

⊥(T.N.D.) Advanced Light Source, Lawrence Berkeley National Laboratory, 6 Cyclotron Rd, Berkeley, CA 94720, United States.

#(J.C.) Univ. Grenoble Alpes, CNRS, Grenoble INP, Institut NEEL, 38000 Grenoble, France.

∇(R.v.G) Surface Preparation Laboratory, Penningweg 69-F, 1507 DE Zaandam, The Netherlands.

Notes

The authors declare no competing financial interest.

ACKNOWLEDGMENT

We acknowledge fruitful discussions with C. Busse. This work was funded by the Deutsche Forschungsgemeinschaft (DFG, German Research Foundation) Projektnummer 278162697∂SFB 1242.

REFERENCES

(1) Geim, A. K.; Grigorieva, I. V. Van der Waals heterostructures. *Nature* 2013, *499*, 419−425.

(2) Zeller, P.; Günther, S. What are the possible moirépatterns of graphene on hexagonally packed surfaces? Universal solution for hexagonal coincidence lattices, derived by a geometric construction. Graphit

M.; Jarillo-Herrero, P.; Ashoori, R. C. Massive Dirac Fermions and Hofstadter Butterfly in a van der Waals Heterostructure. *Science* 2013, *304*, 1427−1430.

(12) Dean, C. R.; Wang, L.; Maher, P.; Forsythe, C.; Ghahari, F.; Gao, Y.; Katoch, J.; Ishigami, M.; Moon, P.; Koshino, M.; Taniguchi, T.; Watanabe, K.; Shepard, K. L.; Hone, J.; Kim, P. Hofstadter's butterfly and the fractal quantum Hall effect in moirésuperlattices. *Nature* 2003, *497*, 598−602.

(13) Kim, K.; DaSilva, A.; Huang, S.; Fallahazad, B.; Larentis, S.; Taniguchi, T.; Watanabe, K.; LeRoy, J.; MacDonald, A. H.; Tutuc, E. Tunable moirébands and strong correlations in small-twist-angle bilayer graphene. *Proc. Natl. Acad. Sci. U. S. A.* 2017, *114*, 3364−3369.

(14) Cao, Y.; Fatemi, V.; Fang, S.; Watanabe, K.; Taniguchi, T.; Kaxiras, E.; Jarillo-Herrero, P. Unconventional superconductivity on magic-angle graphene superlattices. *Nature* 2018, *556*, 43−50.

(15) Cao, Y.; Fatemi, V.; Demir, A.; Fang, S.; Tomarken, S. L.; Luo, J. Y.; Sanchez-Yamagishi, J. D.; Watanabe, K.; Taniguchi, T.; Kaxiras, E.; Ashoori, R. C.; Jarillo-Herrero, P. Correlated insulator behaviour at half-filling in magic-angle graphene superlattices. *Nature* 2018, *556*, 80−84.

(16) Loginova, E.; Nie, S.; Thurmer, K.; Bartelt, N. C.; McCarty, K. F. Defects of graphene on Ir(111): Rotational domains and ridges. *Phys. Rev. B: Condens. Matter Mater. Phys.* 2009, *80*, 085430.

(17) Hattab, H.; N'Diaye, A. T.; Wall, D.; Jnawali, G.; Busse, C.; van Gastel, R.; Poelsema, B.; Michely, T.; Meyer zu Heringdorf, F.-J.; Horn-von Hoegen, M. Growth temperature dependent graphene alignment on Ir(111). *Appl. Phys. Lett.* 2011, *90*, 141903.

(18) Hattab, H.; N'Diaye, A. T.; Wall, D.; Klein, C.; Jnawali, G.; Coraux, J.; Busse, C.; van Gastel, R.; Poelsema, B.; Michely, T.; Meyer zu Heringdorf, F.-J.; Horn-von Hoegen, M. Interplay of Wrinkles, Strain, and Lattice Parameter in Graphene on Iridium. *Nano Lett.* 2012, *12*, 678−682.

(19) Shaw, C. G.; Fain, S. C., Jr.; Chinn, M. D. Observation of Orientational Ordering of Incommensurate Argon Monolayers on

e. *Phys. Rev. Lett.* 1978, *41*, 955−957.
396 *New J. Phys.* 2014, *16*,
083028.
397(3) Artaud, A.; Magaud, L.; Le Quang, T.; Guisset, V.; David, P.;
398 Chapelier, C.; Coraux, J. Universal classification of twisted, strained
399 and sheared graphene moirésuperlattices. *Sci. Rep.* 2016, *6*, 25670.
400(4) Zeller, P.; Ma, X.; Günther, S. Indexing moirépatterns of metal-
401 supported graphene and related systems: strategies and pitfalls. *New J.*
402 *Phys.* 2017, *19*,
013015.
403 (5) Kim, K.; Yankowitz, M.; Fallahazad, B.; Kang, S.; Movva, H. C.
404 P.; Huang, S.; Larentis, S.; Corbet, C. M.; Taniguchi, T.; Watanabe,
405 K.; Banerjee, S. K.; LeRoy, B. J.; Tutuc, E. Waals Heterostructures
406 with High Accuracy Rotational Alignment. *Nano Lett.* 2016, *16*,
407
1989−1995.
408(6) Park, C.-H.; Yang, L.; Son, Y.-W.; Cohen, M. L.; Louie, S. G.
409 Anisotropic behaviours of massless Dirac fermions in graphene under
410 periodic potentials. *Nat. Phys.* 2008, *4*, 213−217.
411(7) Pletikosić, I.; Kralj, M.; Pervan, P.; Brako, J.; Coraux, J.; N'Diaye,
412 A. T.; Busse, C.; Michely, T. Dirac Cones and Minigaps for Graphene
413 on Ir(111). *Phys. Rev. Lett.* 2009, *102*, 056808.
414 (8) Yankowitz, M.; Xue, J.; Cormode, D.; Sanchez-Yamagishi, J. D.;
415Watanabe, K.; Taniguchi, T.; Jarillo-Herrero, P.; Jacquod, P.; LeRoy,
416B. Emergence of superlattice Dirac points in graphene on hexagonal
417boron nitride. *Nat. Phys.* 2012, *8*, 382−386.
418 (9) Li, G.; Luican, A.; Lopes dos Santos, J. M.; Castro Neto, A. H.;
419Reina, A.; Kong, J.; Andrei, E. Y. Observation of Van Hove
420singularities in twisted graphene layers. *Nat. Phys.* 2010, *6*, 109−113.
421 (10) Brihuega, I.; Mallet, P.; Gonzalez-Herrero, H.; Trambly de
422Laissardiere, G.; Ugeda, M. M.; Magaud, L.; Gomez-Rodriguez, J. M.;
423Yndurain, F.; Veuillen, J. Y. Unraveling the Intrinsic and Robust
424Nature of van Hove Singularities in Twisted Bilayer Graphene by
*425*Scanning Tunneling Microscopy and Theoretical Analysis. *Phys. Rev.*
426*Lett.* 2012, *109*, 196802.
427 (11) Hunt, B.; Sanchez-Yamagishi, J. D.; Young, A. F.; Yankowitz,
428M.; LeRoy, B. J.; Watanabe, K.; Taniguchi, T.; Moon, P.; Koshino,
464
(20) Scheithauer, U.; Meyer, G.; Henzler, M. A New LEED
465
Instrument for Quantitative Spot Profile Analysis. *Surf. Sci.* 1986, *178*, 466
441−4
467
51.
(21) Horn-von Hoegen, M. Growth of semiconductor layers studied 468
by spot profile analysing low energy electron diffraction − Part 1 + 2. 469
Z. Kristallogr. 1999, *214*, 591−629 and 470
684−721 .
(22) T N'Diaye, A.; Engler, M.; Busse, C.; Wall, D.; Buckanie, N.; 471
Meyer zu Heringdorf, F.-J; van Gastel, R.; Poelsema, B.; Michely, T. 472
Growth of graphene on Ir(111). *New J. Phys.* 473
2009, *11*, 023006.
(23) Preobrajenski, A. B.; Ng, M. L.; Vinogradov, A. S.; Martensson, 474
N. Controlling graphene corrugation on lattice-mismatched sub- 475
strates. *Phys. Rev. B* 2008, 476
78, 073401.
(24) Hermann, K. Periodic overlayers and moirépatters: theoretical 477
studies of geometric properties. *J. Phys.: Condens. Matter* 2012, *24*, 478
21421
0.
479
(25) Man, K. L.; Altman, M. S. Small-angle lattice rotations in 480
graphene on Ru(0001). *Phys. Rev. B: Condens. Matter Mater. Phys.* 481
2011, *84*, 482
235415.
(26) Borca, B.; Barja, S.; Garnica, M.; Minniti, M.; Politano, A.; 483
Rodriguez-Garcia, J. M.; Hinarejos, J. J.; Farias, D.; Vasquez de Parga, 484
L. A.; Miranda, R. Electronic and geometric corrugation of 485
periodically rippled, self-nanostructured graphene epitaxially grown 486
on Ru(0001). *New J. Phys.* 2010, 487
12, 093018.
(27) Coraux, J.; N'Diaye, A. T.; Busse, C.; Michely, T. Structural 488
Coherency of Graphene on Ir(111). *Nano Lett.* 2008, *8*, 565−570. 489
(28) Rogge, P. C.; Thurmer, K.; Foster, M. E.; McCarty, K. F.; 490
Dubon, O. D.; Bartelt, N. C. Real-time observation of epitaxial 491
graphene domain reorientation. *Nat. Commun.* 492
2015, *6*, 6880.
(29) Usachov, D.; Fedorov, A.; Vilkov, O.; Adamchuk, V. K.; 493
Yashina, L. V.; Bondarenko, A.; Saranin, A. A.; Gruneis, A.; Vyalikh, 494
D. V. Experimental and computational insight into the properties of 495
the lattice-mismatched structures: Monolayers of h-BN and graphene 496

497 on Ir(111). *Phys. Rev. B: Condens. Matter Mater. Phys.* 2012, *86*,
498 155151.

499 (30) N'Diaye, A. T.; Coraux, J.; Plasa, T. N.; Busse, C.; Michely, T.
500 Structure of epitaxial graphene on Ir(111). *New J. Phys.* 2008, *10*,
501 043033.

502 (31) In real space imaging techniques like scanning tunneling
503 microscopy the experiment is sensitive to the moiréangle $\theta_{Gr,moire}$;
504 (32) Halvorson, J. J.; Wimber, R. T. Thermal Expansion of Iridium
505 at High Temperatures. *J. Appl. Phys.* 1972, *43*, 2519−2522.
506 (33) Wimber, R. T. High-temperature thermal expansion of iridium
507 (revised results). *J. Appl. Phys.* 1976, *47*, 5115.
508 (34) Sahin, H.; Cahangirov, S.; Topsakal, M.; Bekaroglo, E.; Akturk,
509 E.; Senger, R. T.; Ciraci, S. Monolayer honeycomb structures of
510 group-IV elements and III-V binary compounds: First-principles
511 calculations. *Phys. Rev. B* 2009, *80*, 155453.
512 (35) Wang, S. Studies of Physical and Chemical Properties of Two-
513 Dimensional Hexagonal Crystals by First-Principles Calculation. *J.*
514 *Phys. Soc. Jpn.* 2010, *79*, 064602.
515 (36) Jean, F.; Zhou, T.; Blanc, N.; Felici, R.; Coraux, J.; Renaud, G.
516 Effect of preparation on the commensurabilities and thermal
517 expansion of graphene on Ir(111) between 10 and 1300 K. *Phys.*
518 *Rev. B: Condens. Matter Mater. Phys.* 2013, *88*, 165406.
519 (37) Nelson, J. B.; Riley, D. P. Thermal Expansion of Graphite from
520 15 to 800 °C.: Part I Experimental. *Proc. Phys. Soc.* 1945, *57*, 477−
521 486.
522 (38) Tsang, D. K. L.; Marsden, B. J.; Fok, S. L.; Hall, G. Graphite
523 thermal expansion relationship for different temperature ranges.
524 *Carbon* 2005, *43*, 2902−2906.
525 (39) In ref 17, a graphene lattice parameter $a_{Gr/Ir}(111)$ = 2.462 Å was
526 determined. This result must be corrected to w$a_{Gr/Ir}(111)$ = 2.465 Å
527 when considering reliable high temperature data for the Ir lattice
528 parameter from refs 30 and 31.
529 (40) Merino, P.; Švec, M.; Pinardi, A. L.; Otero, G.; Martín-Gago, J.
530 A. Strain-Driven MoiréSuperstructures of Epitaxial Graphene on
531 Transition Metal Surfaces. *ACS Nano* 2011, *7*, 5627−5634.
532 (41) Meng, L.; Wu, R.; Zhang, L.; Li, L.; Du, S.; Wang, Y.; Gao, H.-J.
533 Multi-oriented moirésuperstructures of graphene on Ir(111):
534 experimental observations and theoretical models. *J. Phys.: Condens.*
535 *Matter* 2012, *24*, 314214.
536 (42) Novaco, A. D.; McTague, J. P. Orientational Epitaxy ∂ the
537 Orientational Ordering of Incommensurate Structures. *Phys. Rev. Lett.*
538 1977, *38*, 1286−1289.
539 (43) Diehl, R. D.; McGrath, R. Structural studies of alkali metal
540 adsorption and coadsorption on metal surfaces. *Surf. Sci. Rep.* 1996,
541 *23*, 43−171.
542 (44) Caragiu, M.; Finberg, S. Alakali metal adsorption on graphite: a
543 review. *J. Phys.: Condens. Matter* 2005, *17*, R995−R1024.
544 (45) Hooks, D. E.; Fritz, T.; Ward, M. D. Epitaxy and Molecular
545 Organization on Solid Substrates. *Adv. Mater.* 2001, *13*, 227−241.
546 (46) Hamäläinen, S. K.; Boneschanscher, M. P.; Jacobse, P. H.;
547 Swart, I.; Pussi, K.; Moritz, W.; Lahtinen, J.; Liljeroth, P.; Sainio, J.
548 Structure and local variations of the graphene moiréon Ir(111). *Phys.*
549 *Rev. B* 2013, *88*, No. 201406(R).
550 (47) Süle, P.; Szendrő, M.; Hwang, C.; Tapasztó, L. Rotation
551 misorientated graphene moirésuperlattices on Cu (1 1 1): Classical
552 molecular dynamics simulations and scanning tunneling microscopy
553 studies. *Carbon* 2014, *77*, 1082−1089.
554 (48) Tetlow, H.; Posthuma de Boer, J.; Ford, I. J.; Vvedensky, D. D.;
555 Coraux, J.; Kantorovich, L. Growth of Epitaxial Graphene: Theory
556 and Experiment. *Phys. Rep.* 2014, *542*, 195−295.
557 (49) Kozlov, S. M.; Viñes, F.; Görling, A. Bonding Mechanisms of
558 Graphene on Metal Surfaces. *J. Phys. Chem. C* 2012, *116*, 7360−7366.
559 (50) Murata, Y.; Starodub, E.; Kappes, B. B.; Ciobanu, C. V.; Bartelt,
560 N. C.; McCarty, K. F.; Kodambaka, S. Orientation-dependent work
561 function of graphene on Pd(111). *Appl. Phys. Lett.* 2010, *97*, 143114.
565 (52) Nguyen, V. L.; Shin, B. G.; Duong, D. L.; Kim, S. T.; Perello,
565 D.; Lim, J. Y.; Yuan, Q. H.; Ding, F.; Jeong, H. Y.; Shin, H. S.;
Lee, S. 566
M.; Chae, S. H.; Vu, Q. A.; Lee, Y. H. Seamless Stitching of
Graphene 567
Domains on Polished Copper (111) Foil. *Adv. Mater.* 2015,
27, 568
1376−13 569
82.

(51) Nie, S.; Wofford, J. M.; Bartelt, N. C.; Dubon, O. D.; McCarty, K. F. Origin of the mosaicity in graphene grown on Cu(111). *Phys. Rev. B: Condens. Matter Mater. Phys.* 2011, *84*, 155425.